Thermally induced self-locking of an optical cavity by overtone absorption in acetylene gas

P. Dubé, L.-S. Ma,* J. Ye, P. Jungner,† and J. L. Hall

JILA, University of Colorado and National Institute of Standards and Technology, Boulder, Colorado 80309-0440

Received September 15, 1995; revised manuscript received March 4, 1996

Strong self-locking phenomena are observed when laser power is converted into heat by a weakly absorbing medium within a high-finesse cavity. Deposited heat leads to increased temperature and, for the case of weakly absorbing intracavity gases studied here, to an associated reduction of density and refractive index. This thermal change in refractive index provides self-acting cavity tuning near resonant conditions. In the experiments reported here a Fabry–Perot cavity of finesse 274 was filled with acetylene gas and illuminated with a titanium:sapphire laser tuned to the $P(11)$ line of the $\nu_1 + 3\nu_3$ overtone band near 790 nm. The dependencies of maximum frequency-locking range on gas pressure, laser power, and laser frequency sweep rate and direction were measured and could be well unified by analysis based on the thermal model. In the domain of strong self-tuning an interesting self-sustained oscillation was observed, with its several sharp frequencies directly and quantitatively linked to the acoustic boundary conditions in our cylindrical cell geometry. The differences between the behavior of acetylene near 790 nm and molecular oxygen with electronic transition near 763 nm are instructive; whereas the absorbed powers were similar, they differed strongly in their rates for internal to translational energy conversion by collisional relaxation. © 1996 Optical Society of America.

1. INTRODUCTION

External optical resonators can easily build up a laser output power by 2 or 3 orders of magnitude. Recently this property has been exploited to yield saturated absorption signals on weak vibrational overtone transitions of acetylene (C_2H_2).[1] Such vibration–rotation transitions are of current interest because they provide a large number of narrow resonances in the near-infrared[2] and visible[3] wavelength regions for laser frequency stabilization.

The large circulating intensities in the optical resonator required for saturating overtone transitions can cause thermally induced changes in the intracavity gas density and molecular level populations, leading to observable changes in the refractive index of the gas despite the small absorption coefficients. As a result, the cavity resonance frequencies become dependent on the built-up optical field. Venkatesan *et al.*[4] utilized this property to shorten optical pulses by letting the radiation self-sweep a Fabry–Perot resonance across the laser frequency in a time short compared with the original pulse length. Their absorbing medium was a glass filter. Asymmetric resonance profiles from a high-finesse Fabry–Perot cavity filled with a few Torr of acetylene gas were observed by Nakagawa *et al.*[5] when their continuous-wave neodymium:YAG laser was tuned near an overtone transition. The asymmetry was attributed to a shift in cavity resonance frequency resulting from gas heating.

The present study was initially motivated by the observation of spontaneous self-locking of a cavity resonance to an incident laser frequency. Figure 1 shows the transmitted intensity of a Fabry–Perot interferometer filled with 20 Torr of acetylene and illuminated with 140 mW of power from a titanium:sapphire laser tuned to a rotational transition in the $\nu_1 + 3\nu_3$ band of acetylene near 790 nm. The nearly constant transmission over a time of 100 s demonstrates the ability of the cavity to lock its resonance (close) to the frequency of a free-running laser because of thermal adjustment of the refractive index of the gas. Without locking, the laser frequency will drift across the cavity resonance in less than a second. The interferometric power buildup was a maximum of ≈20.

In this paper we report a detailed set of experimental observations covering the influence of gas pressure, laser frequency sweeping direction, and sweeping rate on the Fabry–Perot transmission. We investigated the role played by collisional relaxation rates by replacing acetylene with oxygen. (Molecular oxygen has a magnetic-dipole electronic transition near 763 nm and a slow collisional relaxation rate compared with that of acetylene.) Under certain conditions of laser input power, acetylene gas pressure, and detuning from line center, large amplitude oscillations were observed in transmission. Simple models are given to explain the observations presented. Note that for the pressures used in this paper for demonstrating self-locking (≥4 Torr) there is a negligible degree of saturation of the overtone transitions.

2. EXPERIMENTAL APPARATUS AND MEASUREMENT METHOD

A schematic diagram of the apparatus is shown in Fig. 2. The titanium:sapphire laser designed at JILA provided ≈150 mW of power at 790 nm (120 mW at 763 nm) at the Fabry–Perot input mirror. The titanium:sapphire laser's frequency was monitored with a traveling lambdameter. The single-mode output was adjusted with the following intracavity optics: a three-plate birefringent tuner, a Mach–Zehnder interferometer, and a Brew-

0740-3224/96/0902041-14$10.00

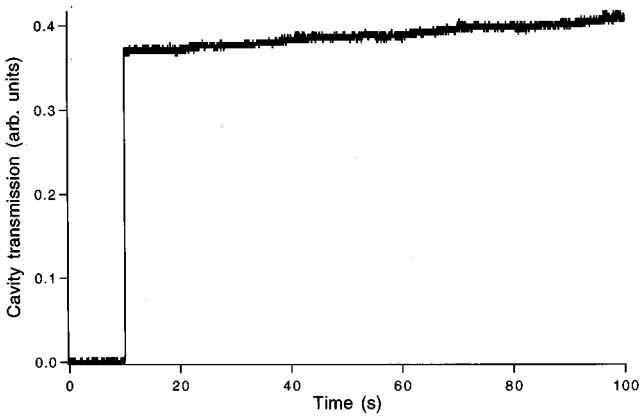

Fig. 1. Demonstration of cavity self-locking to the laser frequency obtained by shining 140 mW of power from a free-running titanium: sapphire laser onto a Fabry–Perot cavity of finesse 274 filled with 20 Torr of acetylene gas. The laser was tuned near the $P(11)$ line center of the $\nu_1 + 3\nu_3$ overtone band of acetylene at 790.7 nm. The slow, upward trend indicates a frequency drift of the laser toward higher frequencies.

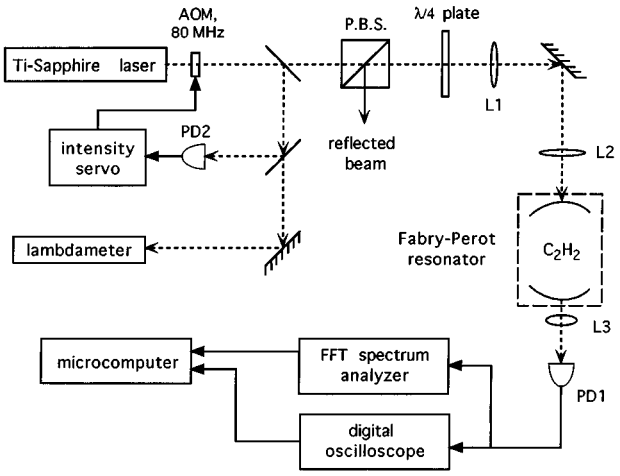

Fig. 2. Experimental configuration. The laser was intensity stabilized, and its free-running noise linewidth was ≤1 MHz. Sweep rates were adjustable. With 140 mW of incident laser radiation the Fabry–Perot cavity built up 10 W of circulating power when there was no gas absorption. Cavity transmission was monitored with photodiode PD1, and the signals were recorded with a digital oscilloscope. FFT, fast Fourier transform; L1–L3, lenses; P.B.S., polarizing beam splitter. Photodiode PD2 monitored the laser output for intensity stabilization.

ster plate. With this arrangement, that is, without frequency stabilization to an external reference, the laser linewidth was ≈1 MHz. For the present experiments, we accomplished frequency scanning by rotating the Brewster plate, which provided a maximum tuning range of ~15 GHz. The Mach–Zehnder interferometer path difference was optimized in real time with a servo loop to keep its transmission maximum locked to the laser frequency. To tune the laser frequency to the oxygen transitions, it was necessary to flush the laser cavity with nitrogen gas.

An acousto-optic modulator operated at 80 MHz was located immediately at the laser output for optical isolation. The acousto-optic modulator was also useful for laser output power control. Further optical isolation between the laser source and the highly reflecting interferometer was provided by a polarizing beam splitter followed by a quarter-wave plate.

The Fabry–Perot interferometer consisted of two nearly identical mirrors mounted upon the axis of a fused-quartz cylindrical spacer having a bore diameter of 0.978 cm and a length of 31 cm. As one of the mirrors was mounted upon a piezoelectric translator, the actual mirror spacing was 33 cm, which gave a free spectral range (FSR) of 455 MHz for the empty cavity. The concave mirrors had a 60-cm radius of curvature, resulting in a beam waist of $w_0 = 0.260$ mm and a mode volume of 35 mm^3. At our main working wavelength of 790 nm the transmission coefficient of each mirror was 0.82%. For the evacuated cavity, the measured finesse was $F = 274$, corresponding to a total cavity loss per round trip of $A_c = 2.29\%$. Thus the power buildup could be a maximum of 63 times. In the 763-nm region, for the study with molecular oxygen, the mirrors' transmission was ≈1.9%, the finesse was 130, and the maximum power buildup was 33 times.

To provide a stable gas environment, we mounted the interferometer inside a vacuum-tight metal cell that could be either attached to a gas-handling system or moved to the optical table. Before filling, the cell was kept under vacuum ($P < 1$ mTorr) with a mechanical pump for several hours to allow for outgassing of the impurities from the cell and Fabry–Perot surfaces. Gas fill pressures at room temperature (298 K) ranged from 4 to 400 Torr.

The results with acetylene gas (Matheson, 99.6%) were obtained with the $P(11)$ line of the $\nu_1 + 3\nu_3$ overtone band at 790.703 nm, which has a line strength of $\approx 7.1 \times 10^{-12}$ cm^2 s^{-1} and a full width collision-broadening coefficient of 11.0(4) MHz/Torr (Ref. 6; 1 Torr = 133 Pa). For oxygen (Scott Specialty Gases, 99.6%), results were obtained with the $^PQ(9, 8)$ line at 763.729 nm,[7] which belongs to the so-called A band, the $b\ ^1\Sigma_g^+ - X\ ^3\Sigma_g^-$ electronic transition. This line has a measured line strength of 4.49 (18) $\times 10^{-12}$ cm^2 s^{-1} and a broadening coefficient of 3.7 MHz/Torr (FWHM).[8]

As shown in Fig. 2, the cavity transmission was detected. The photodiode current was converted to a voltage and sent to either a digital oscilloscope or a fast-Fourier-transform spectrum analyzer, and the data were stored on a microcomputer for subsequent analysis.[9] With the oscilloscope the time evolution of the cavity transmission in response to a swept optical frequency was recorded. Consequently the signals from the cavity transmission were simultaneously functions of time and optical frequency. For ease of comparison among the various data reported in this paper, the time base of the graphs was always converted to frequency from a knowledge of the laser frequency sweeping rate.

3. RESULTS

A. Observation of Asymmetric Cavity Resonances

Figure 3(a) shows the cavity transmission modified by the $P(11)$ line of the $\nu_1 + 3\nu_3$ band of acetylene for a gas pressure of 20 Torr. In the present case the cavity en-

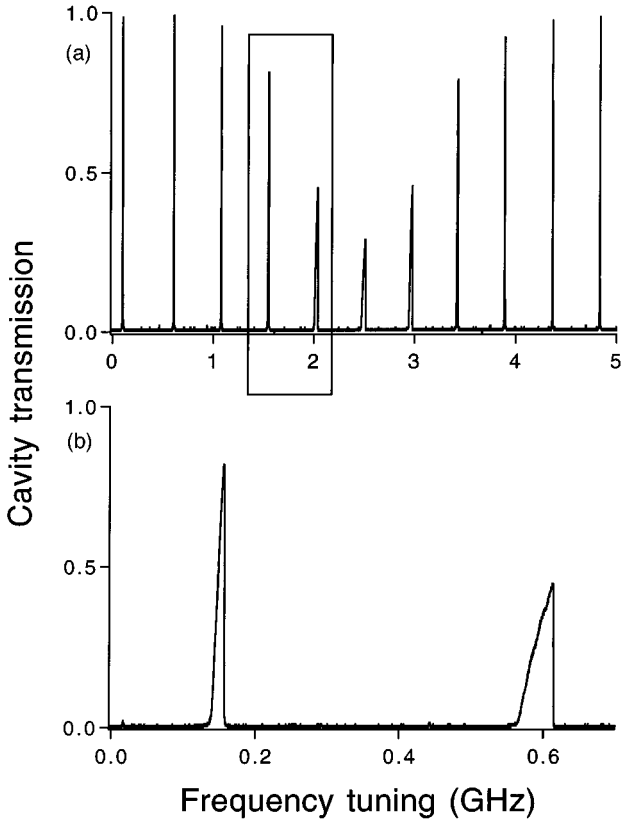

Fig. 3. (a) Cavity transmission as a function of laser frequency over 11 consecutive cavity resonance modes. In this blue scan the $P(11)$ absorption line shape for an acetylene pressure of 20 Torr is outlined by the reduced transmission maxima. Note that the effective absorption path length ($2FL/\pi$, where L is the cavity length) decreases with gas absorption, resulting in a broader observed linewidth. (b) Close-up of two cavity modes illustrating the change in the transmission widths caused by molecular absorption. For these figures the laser power was 140 mW and the sweeping rate was ~10 GHz/s. The cavity transmission given in this figure and the following ones (unless otherwise specified) gives the ratio of transmission with and without gas absorption. It should not be confused with overall cavity transmission, which is limited to 51% at 790 nm for the present cavity when empty.

hanced the absorption at line center by a factor of ≈70, to 71% from the single-pass value of 1%. The widths of the cavity resonances were found to vary across the molecular absorption profile, as shown in the close-up given in Fig. 3(b), and were maximum near line center. Notice the asymmetry in the cavity transmission profiles, which differs substantially from the usual Lorentzian response of high-finesse resonators.

Asymmetric resonances were also observed by Nakagawa *et al.*[5] near 1.064 μm with a high-finesse cavity (≈18 000) filled with 7 Torr of acetylene. The asymmetry appeared when their neodymium:YAG laser was tuned near the line center of an overtone molecular line.

B. Effect of Frequency Scanning Direction

The cavity resonances appeared either broad or narrow depending on whether the optical frequency was increasing (blue scan) or decreasing (red scan). Figure 4 shows measured cavity transmission profiles for blue and red sweeps obtained with an acetylene pressure of 20 Torr and a laser input power of 165 mW. The blue scan of Fig. 4(a) shows a cavity transmission characterized by a nearly linear increase with optical frequency and by an abrupt interruption some 81(2) MHz from the onset. For comparison, a calculated cold cavity resonance with round-trip gas absorption (A_g = 0.020) but no other associated phenomenon taken into account is also displayed in Fig. 4(a). In contrast to the measured transmission, this calculated resonance has a Lorentzian line shape and a 3.1-MHz linewidth (FWHM).

The red scan of Fig. 4(b) is initially characterized by a very narrow transmission peak of 10 kHz FWHM, located 9.4 MHz above the cold cavity resonance position and followed by a ramp of low intensity. Compared with the 3.1-MHz calculated linewidth, that of the red scan has been reduced 300 times. Correspondingly, for the sweeping rate of 100 MHz/s the transmitted laser power duration was reduced from 30 to 0.1 ms.

We refer to the wide transmission ramp of a blue scan as the self-locking range of the cavity. The transmitted intensity in that range was found to be robust to external perturbations such as mechanical vibrations and fre-

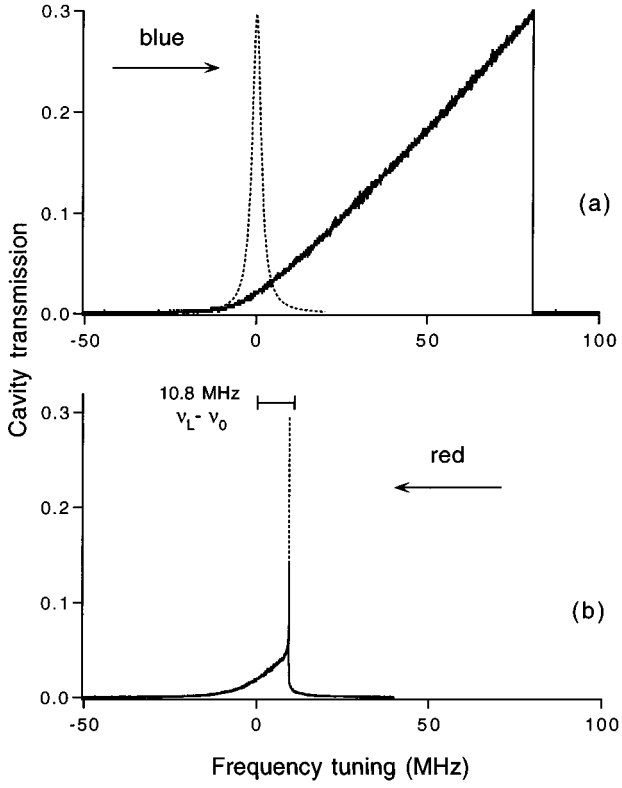

Fig. 4. Cavity transmission for laser sweeping toward a resonance with (a) increasing frequency and (b) decreasing frequency. These scans were obtained near $P(11)$ line center with a laser power of 165 mW, a sweeping rate of 100 MHz/s, and an acetylene pressure of 20 Torr. For comparison, a 3.1-MHz FWHM Lorentzian profile is given in (a). Its width was computed based on round-trip gas absorption at line center (A_g = 0.020) and cavity losses. In (b) the recorded sharp transmission peak is indicated by a dashed line because it was not properly sampled by the oscilloscope. The horizontal 10.8-MHz line gives the calculated position of the transmission spike from the cold cavity line center (cf. Subsection 4.A).

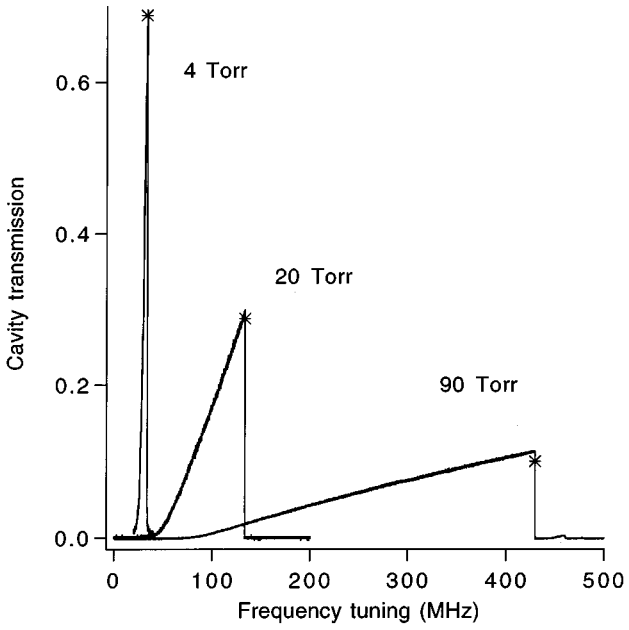

Fig. 5. Blue scans for different acetylene pressures. The laser was tuned near $P(11)$ line center and swept at a rate of 100 MHz/s. Laser powers were 145, 165, and 150 mW for, respectively, pressures of 4, 20, and 90 Torr. The asterisks are computed cavity transmissions for the laser tuned in simultaneous coincidence with $P(11)$ line center and a cavity resonance.

quency instabilities of the laser source. Figure 1 is an example of the transmission as a function of time for the laser tuned in the self-locking region. A slight slope noticeable in Fig. 1 indicates a slow drift of the laser frequency relative to cavity resonance. Stability against cavity drifts is easily determined from the gap between the laser frequency and either extremity of the self-locking range. If we denote the smaller of those gaps by $f_{g'}$ we have for the maximum cavity drift the length $\lambda f_g/(2\,\mathrm{FSR})$.

C. Dependence on Gas Pressure

Figure 5 shows blue scans obtained for several acetylene pressures. The laser was tuned near $P(11)$ line center and delivered 150(10) mW of power at the Fabry–Perot input mirror. In each case the profiles are asymmetric ramps terminating abruptly after some range of frequency sweep. The self-locking regions are 8.5(8), 81(4), and 345(20) MHz wide for pressures of 4, 20, and 90 Torr, respectively. As one would expect, the intensity maximum of each ramp decreases with increasing pressure, owing to gas absorption. This effect is confirmed quantitatively in Fig. 5 by comparison with calculated resonant cavity transmissions, shown as asterisks, which take into account gas absorption at the various pressures [cf. Eqs. 4(b) and 4(c) below]. Gas absorptions were calculated by use of the Voigt function.[10]

D. Dependence on Frequency-Sweeping Rate

We investigated the time response by recording red and blue scans for three different frequency-sweeping rates. These results are shown in Fig. 6 for an acetylene pressure of 90 Torr and a laser frequency tuned near $P(11)$ line center.

For a sweeping rate of 1 GHz/s, the lowest rate reported in Fig. 6, the red and blue scans have the same general features as described above (cf. Fig. 4), i.e., a linear ramp terminating abruptly after 345 MHz for the blue scan and a very narrow transmission peak of 33 kHz for the red scan followed by a low-intensity tail. Increasing the rate tenfold, to 10 GHz/s, narrows the self-locking range from 345 to 210 MHz in the blue scan and broadens the full width at half-maximum of the red scan from 33 to 290 kHz. Finally, at 100 GHz/s, the widths and shapes evolve further, with the blue scan giving a self-locking region of less than 90 MHz and the red scan a transmission width of 1.8 MHz. Notice the almost symmetric profile for the red scan at 100 GHz/s. The width is comparable with the calculated line width of 5.2 MHz associated with gas and cavity losses.

These results clearly demonstrate the existence of a finite time response of the gas-cavity system and suggest that blue and red scan profiles would become essentially identical with still higher sweeping rates, approaching the Lorentzian cavity line shape. (Eventually the simple cavity line shape will show further modification because of transient energy storage, even for the empty cavity, but this phenomenon is not important for the present discussion.)

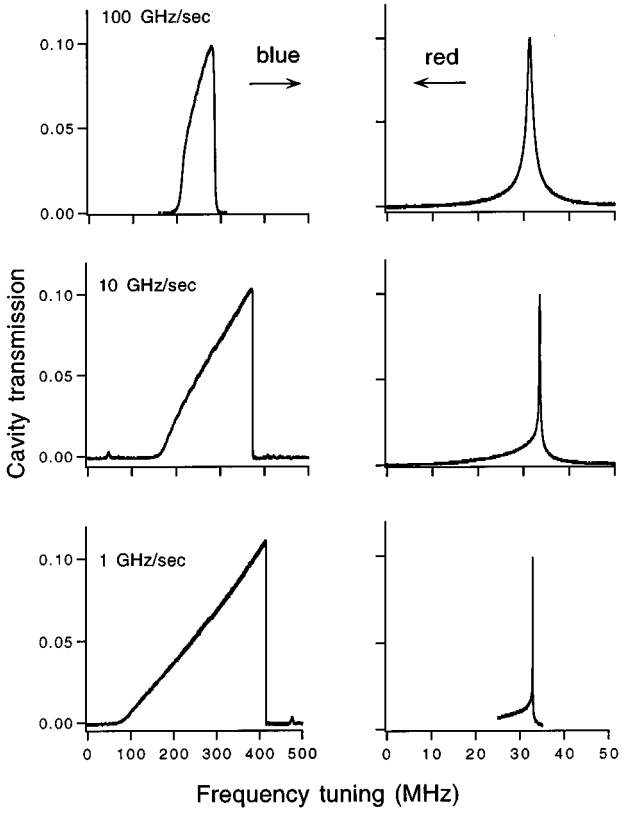

Fig. 6. Blue and red scans across a cavity resonance for three sweeping rates. The laser was tuned near $P(11)$ line center and delivered ~140 mW of power on the cavity filled with 90 Torr of acetylene.

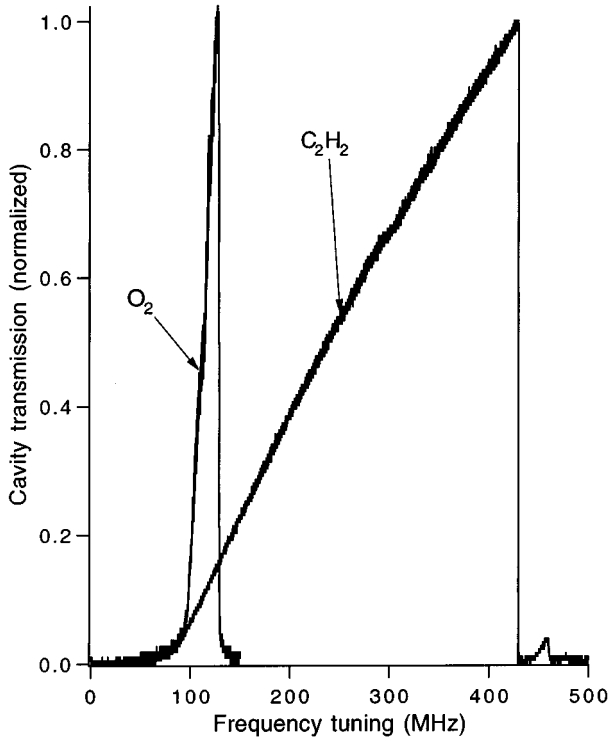

Fig. 7. Comparison of self-locking behavior obtained with 90 Torr of oxygen or acetylene in the Fabry–Perot cavity. For oxygen, laser power near 763 nm was 120 mW; for acetylene, near 790 nm, the power was 150 mW. In both cases the sweeping rates were 100 MHz/s. As discussed in the text, absorption properties are very similar. The large difference in self-locking arises from slow electronic-to-translational energy conversion in the oxygen gas. See Fig. 10 below for the resulting spatial temperature profiles.

E. Comparison between Oxygen and Acetylene

Molecular oxygen has a magnetic-dipole electronic transition in the near infrared known as the A band. This transition possesses several fortuitous features that make oxygen an interesting candidate for comparison with acetylene. First, the strengths of the selected $^{P}Q(9,8)$ line in oxygen and that of the $P(11)$ line in acetylene are comparable (see Section 2). Furthermore, the transition wavelength of $^{P}Q(9,8)$ (763.7 nm) is sufficiently close to the acetylene wavelength (790.7 nm) that the same buildup cavity could be used for both gases.

Blue scans taken with either gas in the Fabry–Perot cavity are combined in Fig. 7. The characteristic ramp followed by a sudden interruption of transmission is also present for oxygen. In each case the gas pressure was 90 Torr, the sweep rate was 100 MHz/s, and the laser was tuned to the respective absorption line center. From transmitted laser power, output mirror reflectivities, and round-trip gas absorptions one finds that the power absorbed in the mode volume is 50(5) mW with acetylene gas and 44(5) mW with oxygen gas. Despite these similarities, the self-locking range with oxygen (35 MHz) is an order of magnitude smaller than that with acetylene (345 MHz). One important difference between these gases, however, is that collisional energy relaxation in oxygen is 4 orders of magnitude smaller than in acetylene.

F. Observation of Acoustic Oscillations

Oscillations in the Fabry–Perot transmitted intensity were observed when the acetylene pressure was increased to 400 Torr. This is illustrated in the blue scan of Fig. 8(a) taken with 140 mW of optical power. Aside from that of high pressure, two other conditions had to be met for sustained oscillations: The input power (P_0) had to exceed ≈110 mW and the laser frequency had to be tuned at least 4 GHz away from $P(11)$ line center when P_0 = 140 mW was used. Except for that of the first ramp, the widths remained constant at 1 FSR throughout the scan, unlike at lower pressure, where the widths were maximized near line center and gradually became narrower with optical detuning (cf. Fig. 3).

Figure 8(b) gives a detailed view of the transmission across two cavity resonances detuned by ~+6 GHz from line center. The first profile is a linear ramp of 900 MHz width at the base, and the second profile has a more complicated dependence on laser frequency and a width of 455 MHz, or 1 FSR. In both cases the oscillations are present only in the last ≈200 MHz of the profiles. Also,

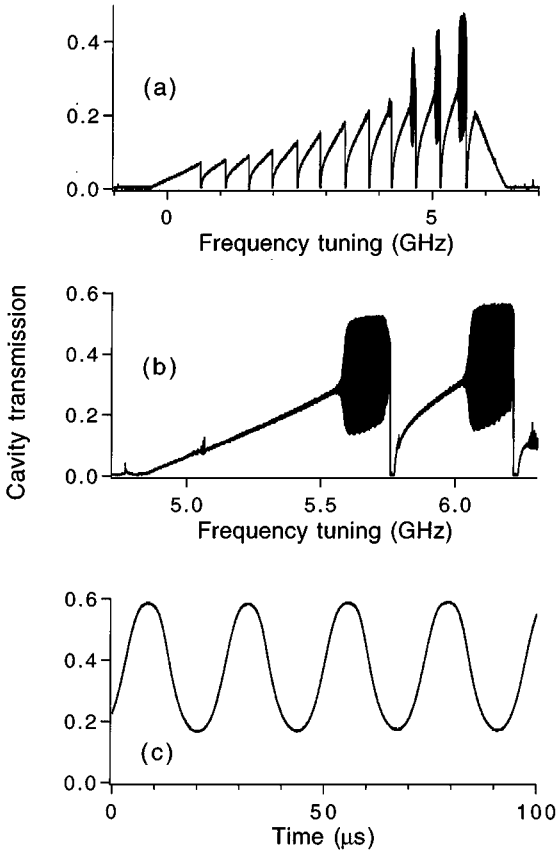

Fig. 8. (a) Blue scan taken with 400 Torr of acetylene and 140 mW of laser power. This scan covered 12 cavity modes. The first ramp coincides with $P(11)$ line center, located at zero detuning. (b) Scan across two cavity modes taken with the laser tuned ~12 FSR's from line center. It shows the region on the transmission ramps where oscillations occurred. (c) Time-resolved record of the 42.5-kHz oscillations observed ~6.5 GHz to the blue from line center.

the maximum light transmission in the range of oscillations exceeds significantly the maximum obtained by projecting the linear portion of the profiles to the interruption point.

A time-resolved record of the intensity fluctuations obtained with fixed laser frequency is shown in Fig. 8(c). It reveals a 42.50(25)-kHz sinusoidal wave form with amplitude comparable with that of average transmission. We investigated the frequency content of this wave form up to 100 kHz by taking its Fourier transform with a fast-Fourier-transform spectrum analyzer; the result is displayed as curve (a) of Fig. 9. The 42.5-kHz component is prominent, as expected from the time record, followed by its second harmonic 25 dB lower (higher harmonics fall outside the span of the spectrum). Other features appear at 11.25 kHz and as 11.25-kHz sidebands on the main peaks; those are due to the dither on the laser's Mach–Zehnder interferometer path difference utilized for operation of its servo loop. We obtained more details on the frequency spectrum of the transmitted light amplitude by tuning the laser frequency slightly below oscillation threshold; the absence of large amplitudes permitted an increase in the sensitivity of the spectrum analyzer. The result is displayed in curve (b) of Fig. 9; only the two features at 11.25 and 42.50 kHz are common to both spectra, but several new ones emerge from the analyzer electronic noise. In particular, higher harmonics from the Mach–Zehnder interferometer dither are now resolved (they are identified by asterisks in Fig. 9), as are features at 8.38, 16.2, 18.8, 25.5, 59.25, 77.75, and 94.75 kHz. Several of these correspond to acoustic resonances within the bore of the Fabry–Perot spacer. The resonance frequencies for a gas inside a circular cylindrical boundary are given by $f_{mn} = (c_s/2a)\alpha_{mn}$, where c_s is the speed of sound, a is the bore radius, and α_{nm} are the roots of $(\mathrm{d}/\mathrm{d}\alpha)J_m(\pi\alpha_{mn}) = 0$ imposed by the boundary condition on the velocity potential at $r = a$.[11] The frequencies are labeled by the integers m and n, which are related to the number of nodal surfaces: m in the azimuthal direction and $n - 1$ in the radial direction. The associated spatial functions are indicated in Fig. 9.

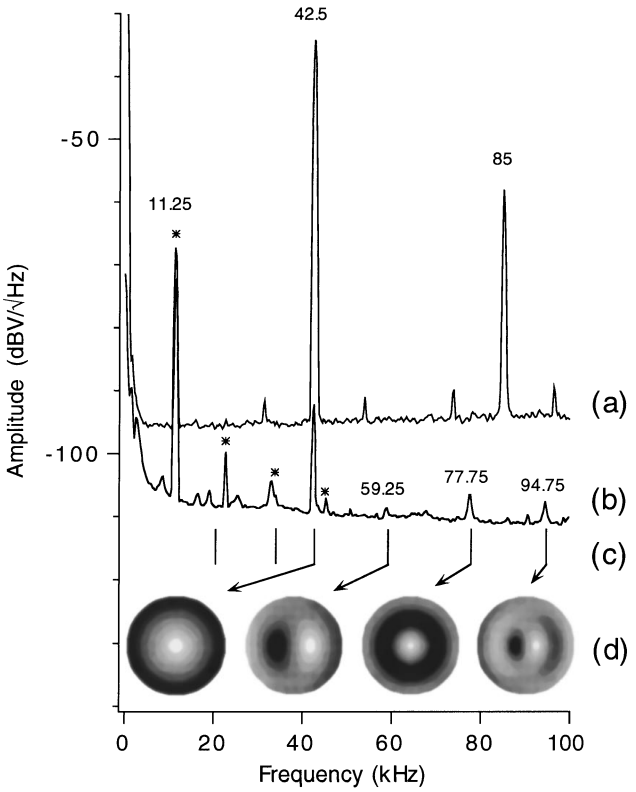

Fig. 9. Frequency spectrum of acoustic resonances in the cavity self-tuning experiment. The experimental conditions were identical to those of Fig. 8. (a) Power above threshold for 42.5-kHz oscillation, showing some second harmonic. One feature at 11.25 kHz and the sidebands arise from intensity AM produced by the laser intracavity Mach–Zehnder servo dither. (b) Spectrum obtained with laser tuned further to the red for near-threshold conditions [cf. Fig. 8(b)]. Lines identified with asterisks are from the étalon dither. (c) Vertical bars show six calculated acoustic eigenmode frequencies based uniquely on the room-temperature speed of sound in acetylene (341 m/s) and the 0.978-cm bore diameter of our cell (cf. Subsection 3.F). In order of increasing frequencies, these eigenmodes are $(m, n) = (1,1)$, (2, 1), (0, 2), (1, 2), (0, 3), (1, 3). (d) Density plots, representing the pressure amplitude across the cavity bore, are given for some of these resonances. Pressure nodes appear as middle gray values, and maxima appear as either light or dark values.

Our spacer has a bore diameter of $2a = 0.978$ cm, and the speed of sound in acetylene at room temperature is 341 m/s,[12] giving $f_{mn} = 34.9\alpha_{mn}$ kHz. A root of special interest here is $\alpha_{02} = 1.2197$, as it gives 42.5 kHz, the frequency of the oscillation in Fig. 8. Note that α_{02} is the lowest-order nonzero root with $m = 0$. Resonance frequencies for other roots are marked with vertical lines in Fig. 9; the features at 59.25, 77.75, and 94.75 kHz are in good agreement with the calculated values. The α_{21} root predicts the existence of a resonance at 33.90 kHz, in accidental coincidence with the third harmonic of the Mach–Zehnder dither frequency. When the spectrum was limited to a few kilohertz near 34 kHz, the resolution was sufficient to permit us to distinguish both features; the acoustic resonance appeared as a 1.25-kHz- (FWHM) wide background, from which protruded a sharp line that was due to the Mach–Zehnder dither. The quality factor of the acoustic resonator is therefore $Q = \nu/\Delta\nu \approx 27$.

We attempted the same experiments by replacing acetylene with 500 Torr of oxygen, but no oscillations were observed in transmission at the expected 41.1 kHz ($c_s = 330$ m/s in oxygen at room temperature[12]).

4. ANALYSIS AND DISCUSSION

The results presented in Section 3 showed how the transmission profiles of a Fabry–Perot cavity could be modified by the presence of a weakly absorbing medium. Aside from a decrease in transmission caused by gas absorption, the cavity transmission revealed asymmetric profiles that depended on the sweep rate, gas pressure, and nature of the gas. Moreover, for appropriate laser input power, gas pressure, and frequency detuning from line center the transmission was found to oscillate at the frequency of an acoustic resonance of the hollow spacer holding the Fabry–Perot mirrors.

At pressures of several Torr the collisional relaxation is expected to convert absorbed radiation mainly into heat. The following analysis of the experimental results is based on the dependence of cavity resonance frequencies on gas heating.

A. Cavity Transmission Profiles: Blue Sweep Direction

We will treat the self-locking phenomenon by first neglecting any radial thermal dependencies. Consider a Fabry–Perot cavity filled with an absorbing gas of refractive index n. For the TEM_{00} mode the optical resonance frequencies are[13]

$$\nu = \frac{c}{2nl}(q + \kappa), \tag{1}$$

where c is the speed of light, l is the mirrors' separation, and q is some integer labeling a longitudinal cavity mode. The effective phase shift κ is a small constant ($\kappa < 1 \ll q$), a known function of the spatial mode and cavity geometry. The dependence of refractive index n on gas density ρ is given by the Gladstone–Dale law:

$$n - 1 = K_{\mathrm{GD}}\rho, \tag{2}$$

where K_{GD} is a quantity that depends on optical wavelength and on the nature of the gas. According to Eqs. (1) and (2), the resonance frequency shift that is due to gas-density change is

$$\Delta\nu = \nu_c - \nu_0 = -\frac{\nu_0}{n}K_{\mathrm{GD}}\Delta\rho, \tag{3}$$

where ν_0 is the resonance frequency of a cavity without gas heating from laser radiation and ν_c is the thermally shifted frequency.

If any element of gas volume is allowed to expand while the gas is heated in the cavity mode, its density (index of refraction) will decrease and the resonance will shift toward higher frequencies, or conversely if the gas is cooled. Therefore frequency scans of the cavity transmission give profiles of a moving resonance, a function of the heat deposited in the mode volume, rather than that of a fixed resonance. This is the basis for describing the response of the cavity transmission to a laser field in the present series of experiments.

We have considered the importance of gas heating on the absorption coefficient, owing to changes in gas density, population distribution, and Doppler width. For our experimental conditions gas heating was estimated to change the absorbed power by less than 1%. Such effects were thus ignored in the analysis. Moreover, it is worth noting that the weak molecular resonances studied in this paper make a negligible contribution to the total index of refraction, which is due to strong electronic transitions in the ultraviolet. The parameter K_{GD} of Eq. (2) can thus safely be assumed constant across the resonance line shapes.

The power absorbed by the gas, P_g, is

$$P_g = A_g P_c = (A_g/t')P_t. \tag{4a}$$

Here A_g is gas absorption per round trip, t' is the output mirror transmission, P_c is the power circulating in the cavity, and P_t is the transmitted power. Equation (4a) is valid regardless of detuning. On resonance, the following equations give the relation between transmitted power (P_{to}) and input power (P_0):

$$P_{to} = 4tt'(F/2\pi)^2 P_0, \tag{4b}$$

with the finesse given by

$$F = \frac{2\pi}{A_c + A_g}. \tag{4c}$$

The symbols have been defined earlier in the text, except for t, which represents the input mirror transmission. $A_c = A + A' + t + t'$ is the cavity losses in terms of the mirrors' absorptions (A, A') and transmissions (t, t'). The unprimed letters refer to the input mirror and the primed letters to the output mirror.

Let us first consider a blue scan obtained by slowly sweeping the laser frequency upward across a resonance of the Fabry–Perot cavity filled with acetylene gas. When light begins to be transmitted through the cavity, a proportional amount is being absorbed by the gas according to Eq. (4a), and the energy is initially stored as overtone vibrational excitation. For steady state (slow sweeping rates) the power leaving the mode volume balances that absorbed. In this case energy can leave the mode volume by radiative decay, diffusion of excited molecules, and heat transfer by either conduction or convection of the energy released as thermal motion during collisions. (Note that, for fast changes in heating rate, some energy would be released as a pressure wave. This case is discussed in Subsection 4.F in the context of acoustic oscillations.) For acetylene, radiative lifetimes are very long [several seconds for the overtone and several milliseconds for single quantum transitions such as between the ground vibrational state and ν_3 (Ref. 14)] compared with collisional relaxation times of ≈ 3 μs at 20 Torr,[15] and they can thus be ignored. We are then left with two main competing processes for energy removal: diffusion of excited molecules and heat transfer. As shown in Subsection 4.D, excited acetylene molecules decay primarily by means of collisions before they can leave the mode volume by diffusion. Hence, in the case of acetylene, we can assume that all the absorbed power P_g is transformed into heat within the mode volume.

In steady state the average temperature in the mode volume (T_m) increases above that of the undisturbed gas or cylinder wall (T_w) until heat transfer equals heat generated. To a good approximation, especially when convection is negligible (see Subsection 4.D), heat flow is proportional to $\Delta T = T_m - T_w$. Consequently ΔT will be directly proportional to power absorbed by the gas, P_g, or the transmitted power, P_t [see Eq. (4a)] as long as the absorption coefficient remains constant.

The mode volume of the Fabry–Perot cavity (≈ 35 mm^3) is far smaller than the total volume of gas, so we can assume that pressure is constant. From the law of perfect gases, with constant pressure, we have $\Delta\rho = -(\Delta T/T_w)\rho$. Using this relation in Eq. (3) gives

$$\Delta\nu = \left(\frac{\nu_0 K_{\mathrm{GD}}}{nT_w}\right)\rho\Delta T, \tag{5}$$

which tells us that frequency shifts in cavity resonance positions are directly proportional to ΔT and therefore to the absorbed and the transmitted powers.

This simple model is in good agreement with the blue scans taken at the slow sweeping rates (≤ 1 GHz/s) of Figs. 4–7, where the linear relationship between $\Delta\nu$ and P_t is observed. Each point on the transmission ramp can be seen as a momentary equilibrium; the detuning be-

tween the shifted cavity resonance (ν_c) and the laser (ν_L), $x = \nu_c - \nu_L$, ensures an absorbed power just sufficient to compensate for the rate of heat loss governed by ΔT. If $\Delta\nu$ is higher than the equilibrium, less power will build up in the cavity, and the gas will cool down until the equilibrium is reached and vice versa. This thermal stabilization mechanism whereby $\nu_c - \nu_L$ is kept constant for a given $\nu_L - \nu_0$ accounts for the self-locking behavior reported in Fig. 1.

The maximum shift $(\Delta\nu)_{\max}$ is obtained when the built-up power reaches its maximum. It occurs with the laser tuned exactly on resonance, $\nu_L = \nu_c$. With further increases in laser frequency, the built-up and absorbed powers can no longer increase; instead they decrease as the laser begins to sample the high-frequency side of the resonance. At this point, even with fixed laser frequency, the cavity resonance is rapidly swept away from the laser frequency because reduced absorbed power leads to gas cooling and reduced buildup, a positive feedback process. The result is a sudden interruption of the transmitted power, observed in all the blue scans reported in this paper.

The width of the self-locking region, $\Delta\nu_{\max}$, is proportional to $\rho\,\Delta T_{\max}$. The other parameters in Eq. (5) can be considered constant for a given gas and molecular absorption line. Within the approximation of linear dependence of temperature increase on absorbed power, the dependence of $(\Delta T)_{\max}$ is then proportional to the absorbed power P_{g0} when the laser is tuned on exact resonance with a mode of the cavity. Combining Eqs. (4a)–(4c), we obtain

$$P_{g0} = \frac{4tA_g}{(A_c + A_g)^2}\,P_0. \tag{6}$$

P_{g0} has a maximum for $A_g = A_c = 0.023$ and is obtained at $P(11)$ line center for an acetylene pressure of ≈25 Torr. The maximum possible fraction of input power absorbed by the gas in the present cavity is $t/A_c = 0.36$.

In Fig. 5 pressures of 4, 20, and 90 Torr gave calculated round-trip absorptions of 0.0047, 0.020, and 0.050, respectively. Equation (6) predicts absorbed powers of 0.20×145, 0.36×165, and 0.31×150 mW for the above pressures, and thus $(\Delta T)_{\max}$ in the ratio 1:2.0:1.6. We can compare these calculated ratios with experimental estimates of $(\Delta T)_{\max}$ based on the self-locking widths of Fig. 5. Replacing $K_{\mathrm{GD}}\rho = n - 1 = 7.74 \times 10^{-7}\ P(\mathrm{Torr})$,[12] $T_w = 298$ K, $\nu_0 = 379$ THz, and $n = 1.00$ in Eq. (5), we obtain $(\Delta T)_{\max} = 1.02\,(\Delta\nu/P)$ K, where $\Delta\nu$ is expressed in megahertz and P in Torr. The experimental results are 2.2(2), 4.1(2), and 3.9(2) K for pressures of 4, 20, and 90 Torr. Their ratios of 1:1.9(2):1.8(2) agree within error bounds with those predicted on the basis of absorbed power with this simple model.

Self-locking ranges increased by a factor of 40, from 8.5 MHz at 4 Torr to 345 MHz at 90 Torr. The main contribution to the self-locking widths is thus from gas density, as we have just determined that temperatures increased by at most a factor of 2 in the same pressure range.

B. Steady-State Model

Inasmuch as we are considering here the cavity transmission line shapes in the case of slow scanning rates, a simple picture for red and blue scans is obtained with a steady-state analysis. Given a laser frequency detuning from resonance, the problem consists of finding the cavity frequency shifts that yield equilibrium between heating and cooling rates in the mode volume. Cooling rates are proportional to temperature increases in the mode volume and frequency shifts, as discussed earlier in this section [see Eq. (5) and the surrounding text]. Actual cooling rates as a function of cavity detunings can be estimated from the ratio of absorbed power at resonance (P_{g0}), as given by Eq. (6), and the measured self-locking ranges $(\nu_c - \nu_0)_{\max}$. Heating rates are simply given by the cavity Lorentzian line shape normalized with the absorbed power at resonance. Combining these results, we can write heat transfer equilibrium in the mode volume as

$$\left[\frac{P_{g0}}{(\nu_c - \nu_0)_{\max}}\right](\nu_c - \nu_0) = \frac{P_{g0}}{1 + \left(\dfrac{\nu_L - \nu_c}{\Delta}\right)^2}, \tag{7}$$

where Δ represents the cavity half-line width. Equation (7) has three roots when one is solving for $\nu_c - \nu_0$. The first, lowest-frequency root gives the small cavity shift obtained when the laser is far detuned. The third root, which lies higher than the laser frequency, corresponds to the self-locking regime. Another solution, given by the second root, lies below the laser frequency but gives a significant detuning of the cavity from its room-temperature equilibrium (unlike the first root). This solution was not observed in our experiments because it is not stable; a slight change of the cavity resonance from the exact equilibrium point would bring the system back to either the first or the third root solution, depending on the sign of the disturbance.

Interesting information is given by the nature of the roots. Transition from real to imaginary is mathematically discontinuous and suggests for the actual gas-cavity system an abrupt change in the position of the cavity resonance frequency while the system seeks a new equilibrium solution. Because the second root is unstable, the system will appear to jump from the first to the third root or vice versa. This description gives a new perspective on the shapes of the transmission profiles in the blue and the red scans. In a blue scan the self-locking solution is initially adopted by the system, until the third root becomes imaginary because the heating can no longer increase. Return of the system to the first root, the only remaining stable solution, causes an abrupt interruption in transmission. For a red scan the system begins with the laser frequency detuned far above cavity resonance. However, for sufficiently small laser detunings, equilibrium of the heating and cooling rates can no longer be achieved by smoothly increasing the cavity resonance frequency because doing so leads instead to a net increase in the heating rates, a runaway process. This is when the first root becomes imaginary, forcing the system to jump to a new equilibrium specified by the third root of the self-locking regime. Such a jump is observed as a sharp spike, followed by a characteristic self-locking ramp in the red scans taken at slow sweeping rates. Equation (7) was solved for the experimental conditions of Fig. 4. The

quantity sought was the laser detuning for which the first root becomes imaginary; it gives the frequency where the bistability occurs and so should predict the position of the spike (in steady state). Figure 4(b) displays the calculated value of 10.8 MHz for direct comparison with the transmission spike at 9.4 MHz. A slight overestimation of the spike position is, however, expected for finite sweeping rates; at the instability threshold the system is still near equilibrium, with cooling practically compensating for heating, thus leading to a soft turn-on and to a shift in the spike position that is due to finite sweeping rates.

C. Dynamic Behavior at Faster Sweep Rates

So far we have considered only slow sweeping rates ($\leqslant$1 GHz/s), which produced scans well described by a steady-state picture. This assumption implied that temperature and density followed closely their steady-state values for the prevailing absorbed power P_g and that the maximum cavity resonance shifts, $\Delta\nu_{\max}$, were observed. In general, however, the internal energy necessary to raise the gas temperature by ΔT, $C\Delta T$ (C being the heat capacity), causes a time lag between ΔT and its steady-state value controlled by the heating and cooling rates. As $\Delta\nu$ also lags [see Eq. (5)], the swept laser frequency reaches the blue, unstable side of the cavity resonance earlier than in steady state. This results in a narrowing in the transmission range of blue scans taken at higher sweep rates, as observed from Fig. 6 with 90 Torr of acetylene. In these experiments the transmission range decreased from 345 MHz for a sweep rate of 1 GHz/s to 85 MHz for 100 GHz/s.

The finite time response of the gas density to absorbed power has also affected the red scans shown in Fig. 6. The frequency width of a transmission peak is determined by the relative sweeping rates of the probing laser and cavity resonance. At one extreme, a slow sweeping laser covers only a small frequency range during the time taken by the cavity resonance to sweep across the laser frequency, resulting in a narrow transmission peak. At the other extreme, of a fast-sweeping laser, the cavity resonance appears to stand still, and the actual profile, free of gas heating effects, is recovered (except for a possible broadening caused by an excessively short interaction time between laser and cavity). We now turn to an analysis that considers rates for conversion of internal energy into heat and permits estimation of gas-temperature distributions within the cavity bore.

D. Self-Locking Ranges and Collisional Relaxation Rates

Subsection 3.E gave a description of blue scans of oxygen and acetylene taken under nearly identical conditions of pressure, sweeping rate, and absorbed power. Despite the similarities of the experimental conditions for the two gases, the self-locking range in oxygen was an order of magnitude smaller than that of acetylene, as shown in Fig. 7.

The temperature increases associated with the self-locking ranges are given by Eq. (5) which is conveniently rewritten in terms of frequency shift ($\Delta\nu$) and gas pressure (P):

$$\Delta T = B(\Delta\nu/P), \tag{8}$$

where B is a constant for a given gas, temperature, and wavelength. In the previous subsection we found that $B(C_2H_2) = 1.02$ Torr K/MHz. For oxygen, replacing $K_{GD}\rho = n - 1 = 3.27 \times 10^{-7}\ P(\text{Torr})$,[12] ν_0=393 THz, $T_w = 298$ K, and $n = 1.00$ in Eq. (5), we obtain $B(O_2) = 2.32$ Torr K/MHz. Note that the values of B differ mostly because the Gladstone–Dale constant of oxygen is 2.4 times smaller than that of acetylene.

In Fig. 7 the self-locking ranges of oxygen and acetylene are 35 and 345 MHz, respectively, for a gas pressure of 90 Torr. Equation (8) gives $\Delta T(O_2) = 0.90(7)$ K and $\Delta T(C_2H_2) = 3.9(2)$ K for the temperature increases at the maximum cavity shifts.

To interpret these results we must consider the energy transfers that control the temperature changes in the mode volume. At gas pressures of several Torr the radiative decay rates of both gases are several orders of magnitude smaller than collisional relaxation rates and will thus be ignored in the discussion. According to Gröber *et al.*,[16] convective motion in enclosed spaces is observed to disappear for Rayleigh numbers (N_{Ra}) below $\approx$1700. Taking the radius of the cavity bore as the characteristic length in our system, we find that $N_{Ra} < 2$ for acetylene pressures of 90 Torr or less and a temperature difference of 4 K. (The numerical values of the physical properties used in the estimation of the Rayleigh number were taken from Ref. 17.) Hence only molecular diffusion and heat conduction will be considered in the following analysis.

The power absorbed by the gas, P_g, is initially stored in excited molecular states: in the $b\,^1\Sigma_g^+$ electronic state of oxygen or in the $\nu_1 + 3\nu_3$ vibrational overtone of acetylene. The spatial distribution of the number density of excited molecules, n^*, is described by the equation of molecular diffusion in cylindrical coordinates. In steady state, considering only a dependence on the radial distance r, the equation is

$$D\frac{d^2n^*}{dr^2} + \frac{D}{r}\frac{dn^*}{dr} - \frac{n^*}{\tau} + f(r) = 0, \tag{9a}$$

with boundary conditions

$$n^*(a) = 0, \quad \frac{dn^*}{dr}(0) = 0, \tag{9b}$$

where a is the bore radius, D is the self-diffusion coefficient, and $f(r)$ is the number of molecules promoted to an excited state per unit volume and time by absorption of the built-up field. This source term is given by the following formula:

$$f(r) = \left(\frac{P_g}{h\nu}\right)\frac{1}{V_{00}}\exp(-2r^2/w_0^2), \tag{10}$$

where $V_{00} = \pi w_0^2 L/2$ is the volume of the TEM_{00} mode. In writing Eqs. (9) and (10) we have ignored the axial dependence of the mode size; it actually varied from w_0 in the center of our cavity to 1.17 w_0 at either mirror. Also, we ignored the weak axial dependence that is due to absorption along the intracavity path.

At any point in the bore of the Fabry–Perot spacer, heat is released at the rate of $h\nu n^*/\tau$, where $h\nu$ is the en-

Table 1. Physical Parameters for the Diffusion and Heat Equations

Parameter	O_2	C_2H_2	Units	References[a]
λ_c	0.0263	0.0214	J m^{-1} s^{-1} K^{-1}	17
DP	0.0154	0.0091	m^2 Torr s^{-1}	17, 18
$1/(\tau P)$	1.32	1.81×10^4	s^{-1} Torr^{-1}	19, 15
P	90	90	Torr	
$h\nu$	2.601×10^{-19}	2.512×10^{-19}	J	
w_0	0.0255	0.0260	cm	
V_{00}	0.0337	0.0350	cm^3	
a	0.489	0.489	cm	
P_g	0.044	0.050	W	

[a] When applicable, references are given in the order of appearance of the numerical values in each row.

ergy stored in one molecule and τ is the energy decay time, the inverse of the collisional decay rate. The solution to Eqs. (9), $n^*(r)$, gives the source term in the heat-conduction equation. Written as a function of the temperature difference $\theta \equiv T(r) - T_w$, this equation in cylindrical coordinates is

$$\lambda_c \frac{d^2\theta}{dr^2} + \frac{\lambda_c}{r}\frac{d\theta}{dr} + \frac{h\nu}{\tau} n^*(r) = 0, \tag{11a}$$

with boundary conditions

$$\theta(a) = 0, \quad \frac{d\theta}{dr}(0) = 0. \tag{11b}$$

λ_c is the thermal conductivity of the gas. Table 1 summarizes the numerical values of the physical parameters relevant to Eqs. (9)–(11). A comparison of the columns indicates that all the like parameters are within a factor of 2 of one another, except for the relaxation rates between internal and kinetic energy; this rate is 4 orders of magnitude larger in acetylene than in oxygen.

Figure 10(a) gives the numerical solutions of $n^*(r)$ for oxygen and acetylene as a function of normalized radial distance r/a. The population distribution of excited acetylene molecules closely follows the intensity profile of the built-up laser field; they would not be distinguishable in the figure. This shows that most acetylene molecules, at a pressure of 90 Torr, are collisionally deexcited in the mode volume before they escape by diffusion. Consequently, the heat generated in acetylene has the same spatial profile as that of the light intensity. In contrast, the distribution of excited oxygen molecules is far broader, which indicates that a significant fraction of excited molecules diffuses out of the mode volume, a consequence of a slow rate for converting internal energy into translational energy. Heat will then be released throughout the bore of the spacer and at the walls.

Figure 10(b) displays the solutions to the heat equation. As expected from the distribution of excited molecules, the temperature increase in oxygen is lower and more uniform in the radial direction than in acetylene. Consider the temperature in the mode volume, averaged over a radius extending up to the $1/e$ intensity of the optical beam ($\xi = w_0/\sqrt{2}$):

$$T_m - T_w = \langle\theta\rangle_m = \frac{4}{w_0^2}\int_0^{\xi} \theta(r) r\,dr. \tag{12}$$

From the numerical solutions reported in Fig. 10(b) we obtain $\langle\theta\rangle_m = 1.0(1)$ K for oxygen and 3.8(4) K for acetylene, in satisfactory agreement with the temperature increases obtained from the self-locking ranges, 0.90(7) and 3.9(2) K, respectively. The discrepancy in both cases is attributed mainly to uncertainty in the absorbed power. For oxygen there is an additional possible reduction in the measured self-locking range caused by a finite sweeping rate of 100 MHz/s. Although the scans of Subsection 3.D reported for acetylene were consistent with a steady-state picture up to sweeping rates of 1 GHz/s, that may not be the case for oxygen. In fact, one expects longer times for reaching steady state in oxygen because its radial temperature gradients in the mode volume are much smaller than in acetylene.

A simple method for determining whether molecular diffusion plays a role in the final temperature distribution is to evaluate the characteristic length $l_c = \sqrt{\tau D}$. Outside the optically pumped mode volume, population density decreases by at least a factor of $1/e$ when the radial distance is incremented by l_c. Thus diffusion becomes important only if l_c/w_0 is of the order of 1 or larger. For example, $l_c/w_0 = 4.7$ for oxygen and $l_c/w_0 = 0.030$ for

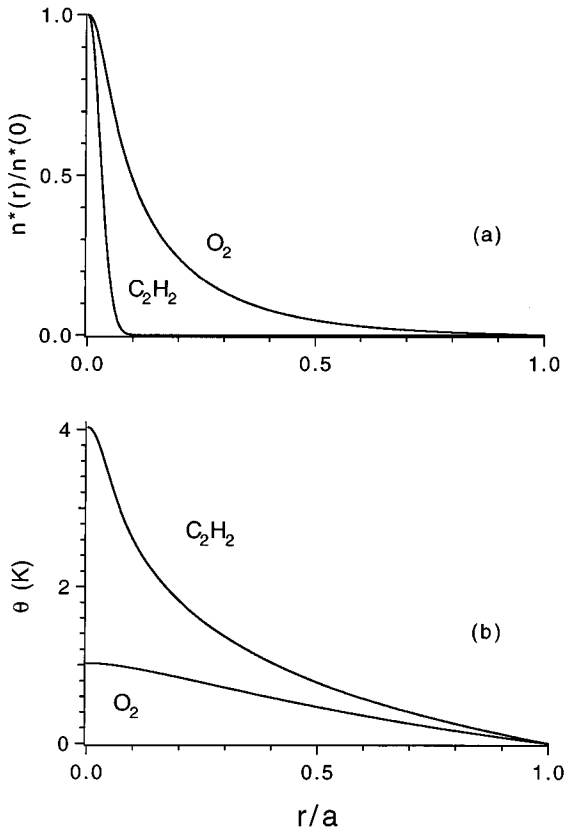

Fig. 10. Calculated excited-state population densities of oxygen and acetylene molecules as a function of distance, from center $r/a = 0$ to wall (a is the bore radius). (b) Temperature profiles for driven heat-diffusion equations, with spatially distributed heat input from (a) above. The relevant parameters are summarized in Table 1.

acetylene. Note that the collisional decay time τ would have to be increased by nearly 1000 times in acetylene before diffusion (at 90 Torr) could affect the temperature distribution and therefore the width of the self-locking range. This explains why the temperature increase in oxygen was not dramatically lower than in acetylene. Rather, it was fortunate that energy relaxation in oxygen was sufficiently slow to allow the effect of diffusion to be clearly observed as a reduction in the self-locking range.

E. Evidence of Thermal Lensing at 400 Torr

The model used so far for describing the self-locking ranges relied on the assumption that transmission was interrupted when the laser was in exact resonance with a cavity mode, because further increases in absorbed power, and therefore in mode volume temperature, by adjustment of the laser-cavity detuning were no longer possible. Consequently, at the interruption point, both absorbed and transmitted powers had reached their maximum values permitted by the cavity.

However, in Subsection 3.F we reported blue scans taken at 400 Torr that had ramps terminating with an average intensity significantly lower than the maximum allowed by the cavity, as emphasized by the oscillations. This observation implies that the maximum temperature increases in the mode volume were lower than expected. The first ramp in Fig. 8(b) has a width of 900 MHz, corresponding to a temperature of 2.3 K according to Eq. (8). On the other hand, for the experimental conditions of Fig. 8(b), i.e., an acetylene pressure of 400 Torr, an optical power of 140 mW, and a detuning of 12 FSR's from $P(11)$ line center, the model of Subsection 4.D predicts that $\Delta T_{\max} = 3.4$ K.

We propose an argument based on thermal lensing to explain the anomaly in the temperature increases ($\Delta T_{\max}$) at 400 Torr. The variation of refractive index with radial distance, $n(r)$, across the bore of the cavity can be calculated from the temperature profile $\theta(r)$ of acetylene. For $\theta(r) \ll T_w$ we have, from the ideal gas law,

$$n(r) - n(0) = K_{\mathrm{GD}}\rho_w\left[\frac{\theta(0) - \theta(r)}{T_w}\right], \tag{13}$$

where $n(0)$ is the index of refraction on the axis and ρ_w is the gas density at room temperature (T_w). To take advantage of the simplicity of paraxial ray analysis, we fitted a Gaussian duct[13,20] to the index-of-refraction profile near the axis. The Gaussian duct is defined as an index of refraction varying quadratically with radial distance:

$$n(r) - n(0) = 1/2 n_2 r^2. \tag{14}$$

For an acetylene pressure of 400 Torr, the fit yields

$$n_2 = 5.4 \times 10^{-4} \Delta T \ \mathrm{cm}^{-2}. \tag{15}$$

The *ABCD* matrix for our cavity, including the diverging Gaussian duct characterized by n_2, was evaluated. From the stability condition for resonators, $|A + D| \leqslant 2$, we find that instability sets in when $n_2 \geqslant 0.00111\ \mathrm{cm}^{-2}$ or, according to Eq. (15), when $\Delta T \geqslant 2.1$ K. This value is in good agreement with the 2.3-K increase deduced from the self-locking range of Fig. 8(b). Therefore the premature interruption of transmission is consistent with the destabilizing effect of the negative thermal lens on the Fabry–Perot resonator. (The assumption of a Gaussian duct, although it describes well the region within the beam waist, is, however, an approximation. Furthermore, the beam waist enlarges when the cavity comes close to instability, thus affecting temperature profiles and n_2.)

There exists a simple connection between cavity resonance shift $\Delta\nu$ and n_2, especially when molecular diffusion can be neglected. In this case, examination of Eqs. 9(a) and 11(a) reveals that the spatial dependence of $\theta(r)$ does not depend on ΔT. This allows us to write the contribution from the temperature profile to n_2 as a constant (β) scaled by the temperature increase in the mode volume, ΔT. Combining Eqs. (13) and (14) with this simplification, we obtain

$$n_2 = \beta \Delta T \frac{K_{\mathrm{GD}}\rho_w}{T_w}. \tag{16}$$

The relation between $\Delta\nu$ and n_2 is immediately obtained from Eqs. (16) and (5):

$$\Delta\nu = (\nu_0/\beta) n_2, \tag{17}$$

which shows that cavity resonance shifts have a one-to-one correspondence with n_2, irrespective of the gas properties, provided that diffusion is neglected and the steady-state temperature distribution prevails. Because the value of n_2 for which the cavity becomes unstable is well defined by geometry, so is the maximum self-locking range.

Thermal lensing also provides an explanation for the constant width of all but the first of the 12 profiles of Fig. 8(a). After the initial ramp, terminated by thermal lensing, the gas cools down and rapidly sweeps the next cavity mode into (detuned) resonance with the laser. The gas remains warmer than room temperature because the self-locking width of the first profile exceeded 1 FSR; this accounts for the distorted ramps that are starting up from a shifted position rather than from equilibrium. Then the second ramp is also terminated by thermal lensing, with same frequency shift from its equilibrium as the first ramp. As long as thermal lensing remains the cause of interruption, the profiles should be separated by 1 FSR.

F. Acoustic Oscillations

As reported in Subsection 3.E (Fig. 8), large amplitude oscillations were observed in transmission for an acetylene gas pressure of 400 Torr. The 42.5-kHz frequency was identified as corresponding to the ($m = 0$, $n = 2$) acoustic mode of the cylindrical Fabry–Perot bore.

For the present system sustained oscillations can derive energy only from the built-up laser field. Neglecting the effects of thermal conductivity, the linear acoustic wave equation for pressure or density has a source term proportional to the time derivative of the heating rate[21]:

$$\frac{\partial}{\partial t}\left(\frac{\delta n^* h\nu}{\tau}\right) \cong \frac{\partial}{\partial t}(\delta P_g), \tag{18}$$

where t is the time, δn^* represents the changes in density n^*, and δP_g is the absorbed power P_g that occurs at the acoustic frequency. The equality suggested in Eq. (18)

between heating rate and absorbed power holds only if the collisional decay time τ is much shorter than a period of oscillation of P_g. For an acetylene pressure of 400 Torr the equality holds because $\tau = 0.14\ \mu s \ll 1/\omega = 3.7\ \mu s$ ($f = 42.5$ kHz). If τ becomes comparable with $1/\omega$, the heating rate lags by 45° from the absorbed power, and the oscillation amplitude decreases by $\sqrt{2}$ (a first-order system). Both changes decrease the ability of the absorbed power to drive an acoustic oscillation; as will be shown below, the phase is ideal when the relaxation time vanishes. For an oxygen pressure of 500 Torr the collision decay time of $\tau = 1500\ \mu s$ is much longer than $1/\omega = 3.9\ \mu s$ ($f = 41.1$ kHz). This results in a small amplitude modulation of the heating rate and a phase lag of ≈90° from an eventual sinusoidal variation in the absorbed power. We believe that this explains why no acoustic oscillations were observed in oxygen with the present experimental conditions.

For a sustained acoustic oscillation the gain must exceed the losses inherent in the resonator. Assuming fast collisional decay rates, valid for a description of the Fabry–Perot cavity filled with 400 Torr of acetylene, we need consider only the relation between absorbed power and density changes to describe the gain characteristics of our system. An acoustic oscillation produces a harmonic time variation of gas density on the cavity axis, $\delta\rho_a \sin(\omega t)$, which causes a change in the cavity resonance frequency $\delta\nu(t)$. From Eq. (3), with $n = 1.00$, we have

$$\frac{\delta\nu(t)}{\nu_0} = -K_{\mathrm{GD}}\delta\rho_a \sin(\omega t). \tag{19}$$

$\delta\nu(t)$ is mapped onto the transmitted and absorbed power according to the cavity line shape. For a Lorentzian profile $L(x = \nu_c - \nu_L)$, and small amplitudes, we obtain the following expression:

$$\delta P_g(t) = P_{g0}\frac{\mathrm{d}L(x)}{\mathrm{d}x}\delta\nu(t) = -\frac{9}{8\sqrt{3}}P_{g0}\frac{\delta\nu(t)}{\Delta}, \tag{20}$$

where Δ is the half-width at half-maximum of the cavity resonance and P_{g0} is the power absorbed on resonance. The derivative of $L(x)$ was evaluated at $x = \Delta/\sqrt{3}$, giving the maximum slope on the low-frequency side of the profile. When Eqs. (18)–(20) are combined, the rate of change of absorbed power becomes

$$\frac{\partial}{\partial t}\delta P_g = \omega\left[\frac{9}{8\sqrt{3}}\nu_0 K_{\mathrm{GD}}\right]\left\{\frac{P_{g0}}{\Delta}\right\}\delta\rho_a \cos\omega t. \tag{21}$$

Equation (21) shows that the source term to the wave equation ($\sim\cos\omega t$) is 90° ahead of the driven term $\delta\rho_a \sin\omega t$. This is the correct phase for maximum power transfer to a harmonic oscillator. As mentioned earlier in this section, the phase shift will change if the collisional relaxation time increases, e.g., if the pressure is lowered.

Gain arises from having a source term proportional to $\delta\rho_a$. For given optical and acoustic frequencies, all the other terms in Eq. (21) are constant, except for the quantity in braces, which depends on gas absorption. Using the definition of finesse, $F = \mathrm{FSR}/2\Delta$, and Eqs. (4c) and (6), we get

$$\left\{\frac{P_{g0}}{\Delta}\right\} = \left[\frac{16\pi t}{\mathrm{FSR}}P_0\right]\frac{A_g}{(A_c + A_g)^3}. \tag{22}$$

This expression has a maximum for round-trip gas losses of $A_g = A_c/2 = 0.0115$. With 400 Torr of acetylene gas in a 33-cm-long cavity the optimum gas absorption is found 5.0 GHz from $P(11)$ line center, representing 11 FSR's. Oscillations were observed only ≈9–≈14 FSR's away from line center, indicating that the system was near threshold. This would account for the absence of oscillations when the input power was lowered from 140 to 110 mW.

As expected for near-threshold conditions, oscillations in Fig. 8(b) occurred only in the region of maximum slope, located at 75% of the resonance cavity transmission. Note that thermal lensing has prevented the laser from exploring the region of lower gain above 75% transmission. The average slope of the Lorentzian decreases with the frequency range covered by an oscillation, thereby limiting the amplitude. Ultimately, the amplitude is clamped at the transmission maximum.

5. SUMMARY AND CONCLUSIONS

Spontaneous self-locking of a Fabry–Perot cavity to the frequency of a built-up laser field was observed when power was absorbed by an intracavity gas. Several experiments were conducted to investigate the origin of the self-locking phenomenon and its dependence on parameters such as gas pressure, laser sweeping direction, laser sweeping rate, and molecular energy relaxation rates. We performed the experiments mainly by filling the resonator with acetylene gas and tuning the laser near the $P(11)$ line of the $\nu_1 + 3\nu_3$ vibrational overtone.

The analysis of the results was based on the dependence of cavity resonance frequencies on the changes in refractive index caused by gas heating. Equation 5 in Subsection 3.A shows that a resonance shift or self-tuning is directly proportional to temperature increase and gas density. Moreover, because convection was found unimportant for our experimental conditions, temperature changes were considered to be directly proportional to absorbed and transmitted powers. As a consequence, self-tuning and transmitted power were proportional to each other, as confirmed by the linear ramps in blue scans. When self-tuning reaches peak resonance condition, temperature can no longer increase, and the self-locking regime collapses. It is the product of absorbed power and gas density (refractive index) that usually determines the width of self-locking. One exception to this rule was found for a pressure of 400 Torr, where the maximum self-locking range was 900 MHz although it should have been 1300 MHz according to the above model. Thermal lensing was believed to be responsible for the early termination in transmission. Using paraxial ray analysis, taking into account the index profile in the mode volume, we calculated the temperature change for instability to be 2.1 K, in good agreement with the 2.3 K deduced from the self-locking range of 900 MHz.

A steady-state analysis of the equilibrium between heating and cooling rates gave a third-order algebraic equation for the cavity resonance shifts. We could predict the features of red and blue scans quantitatively simply by looking at the nature of the roots as a function of laser frequency. In a blue scan, transmission is interrupted when the root describing self-locking becomes imaginary. Similarly, in a red scan the cavity sweeps rapidly across the laser frequency when the root describing the system equilibrium for large laser detunings becomes imaginary. In either case a transition from a real to an imaginary root describes a physical situation in which the equilibrium between heating and cooling rates is no longer possible for that particular evolution of the system.

High sweep rates emphasized the time constant associated with bringing the temperature distribution to steady state. Ramps became curved because temperatures lagged from the equilibria prescribed by absorbed powers. Peaks in red scans were broader because the laser sweeping rate was comparable with the time taken by the absorbed power in the gas to be converted into a temperature distribution.

A quantitative analysis of the temperature changes in the mode volume required solving for temperature distributions across the bore of the cavity. This analysis was motivated by the role played by energy relaxation rates in determining the self-locking widths observed with acetylene and oxygen. The only energy transfer mechanisms found important were molecular diffusion and energy relaxation. The calculations predicted the observed temperature changes. With oxygen, a significant fraction of excited molecules left the mode volume by diffusion and released their electronic energy throughout the bore and at the wall. With acetylene, essentially all the molecules released their overtone excitation as heat in the mode volume, where they had been excited.

Sustained acoustic oscillations at 42.5 kHz were observed with 400 Torr of acetylene and only for transmission exceeding ≈50% of the maximum and for detunings of ≈5 GHz from $P(11)$ line center. These particularities were accounted for by consideration of the gain mechanism for a density wave driven by a heat source. (Although other rotational lines were not studied, oscillations should be observed for any line having sufficient line-center absorption for optimum conversion of laser power into an acoustic gain.)

The self-locking phenomenon described here is not limited to acetylene or oxygen as an absorber. Whenever heating can cause a change in the optical path of a resonator, self-locking should be expected. An interesting example, observed in our laboratory, is that of a superhigh-finesse cavity ($F > 10{,}000$) capable of building up a modest laser power, say, 100 mW, into ~100 W. The infinitesimal fraction of power absorbed by the low-loss mirrors turned out to be significant with such high circulating powers, causing observable self-locking.

ACKNOWLEDGMENTS

This study is an outgrowth of research sponsored at JILA in part by the National Institute of Standards and Technology as part of its program of technology development for prospective fundamental standards and in part by the U.S. Office of Naval Research, the U.S. Air Force Office of Scientific Research, and the National Science Foundation. P. Dubé thanks the Natural Sciences and Engineering Research Council of Canada for a postdoctoral scholarship during the course of this study.

*Permanent address, Department of Physics, East China Normal University, Shanghai, China.

†Present address, Laboratory of Physical Chemistry, University of Helsinki, Helsinki, Finland.

REFERENCES AND NOTES

1. M. de Labachelerie, K. Nakagawa, and M. Ohtsu, "Ultranarrow $^{13}C_2H_2$ saturated-absorption lines at 1.5 μm," Opt. Lett. **19**, 840–842 (1994).
2. K. Nakagawa, M. de Labachelerie, Y. Awaji, M. Kourogi, T. Enami, and M. Ohtsu, "Highly precise 1-THz optical frequency-difference measurement of 1.5-μm molecular absorption lines," Opt. Lett. **20**, 410–412 (1995).
3. L.-S. Ma, P. Dubé, P. Jungner, J. Ye, and J. L. Hall, "Saturation spectroscopy of molecular overtones for laser frequency standards in visible and near-visible domains," in *Quantum Electronics and Laser Science Conference*, Vol. 16 of 1995 OSA Technical Digest Series (Optical Society of America, Washington, D.C., 1995), p. 18.
4. T. N. C. Venkatesan, H. M. Gibbs, S. L. McCall, A. Passner, A. C. Gossard, and W. W. Wiegman, "Optical pulse tailoring and termination by self-sweeping of a Fabry-Pérot cavity," Opt. Commun. **31**, 228–230 (1979).
5. K. Nakagawa, T. Katsuda, A. S. Shelkovnikov, M. de Labachelerie, and M. Ohtsu, "Highly sensitive detection of molecular absorption using a high finesse optical cavity," Opt. Commun. **107**, 369–372 (1994).
6. F. S. Pavone, F. Marin, M. Inguscio, K. Ernst, and G. Di Lonardo, "Sensitive detection of acetylene absorption in the visible by using a stabilized AlGaAs diode laser," Appl. Opt. **32**, 259–262 (1993).
7. D. E. Burch and D. A. Gryvnak, "Strengths, widths, and shapes of the oxygen lines near 13,100 cm^{-1} (7620 Å)," Appl. Opt. **8**, 1493–1499 (1969).
8. J. H. Miller, R. W. Boese, and L. P. Giver, "Intensity measurements and rotational intensity distribution for the oxygen A-band," J. Quant. Spectrosc. Radiat. Transfer **9**, 1507–1517 (1969).
9. Oscilloscope, LeCroy Model 9410; FFT spectrum analyzer, Stanford Research Systems SR760. This information is provided for the purpose of technical completeness and not as a product or company endorsement.
10. B. H. Armstrong, "Spectrum line profiles: the Voigt function," J. Quant. Spectrosc. Radiat. Transfer **7**, 61–88 (1967).
11. P. M. Morse and F. Feshbach, *Methods of Theoretical Physics* (McGraw-Hill, New York, 1953), parts I and II.
12. L'Air Liquide, Division Scientifique, *Encyclopédie des Gaz* (Elsevier/North-Holland, New York, 1976).
13. A. E. Siegman, *Lasers* (University Science Books, Mill Valley, Calif. 1986).
14. C. P. Rinsland, A. Baldacci, and K. N. Rao, "Acetylene bands observed in carbon stars: a laboratory study and an illustrative example of its application to IRC+10216," Astrophys. J. Suppl. Ser. **49**, 487–513 (1982).
15. J. D. Lambert and R. Salter, "Vibrational relaxation in gases," Proc. R. Soc. London Ser. A **253**, 277–288 (1959).
16. H. Gröber, S. Erk, and U. Grigull, *Fundamentals of Heat Transfer* (McGraw-Hill, New York, 1961), Chap. 14, p. 317.
17. D. R. Lide, ed., *CRC Handbook of Chemistry and Physics*, 74th ed. (CRC, Boca Raton, Fla., 1993–1994).
18. The self-diffusion coefficient of C_2H_2 at room temperature was calculated based on the average cross section obtained from thermal conductivity and viscosity. Numerical values

for these properties were taken from Ref. 17.
19. L. R. Martin, R. B. Cohen, and J. F. Schatz, "Quenching of laser induced fluorescence of O_2 ($b^1\Sigma_g^+$) by O_2 and N_2," Chem. Phys. Lett. **41**, 394–396 (1976).
20. H. Kogelnik and T. Li, "Laser beams and resonators," Appl. Opt. **5**, 1550–1567 (1966).
21. R. T. Bailey, F. R. Cruickshank, R. Guthrie, D. Pugh, and I. J. M. Weir, "Short time-scale effects in the pulsed source thermal lens," Mol. Phys. **48**, 81–95 (1983); M.-C. Gagné and S. L. Chin, "Energy relaxation time in a gas mixture measured by a photothermal probe beam deflection technique," Appl. Phys. B **52**, 352–358 (1991).